Temperature Dependence of Avalanche Breakdown of AlGaAsSb and AlInAsSb Avalanche Photodiodes

Bingtian Guo, Sheikh Z. Ahmed, Xingjun Xue, Ann-Kathryn Rockwell, Jaedu Ha, Seunghyun Lee, Baolai Liang, Andrew H. Jones, J. Andrew McArthur, Sri H. Kodati, Theodore J. Ronningen, Sanjay Krishna, *Fellow, IEEE*, Jong Su Kim, Seth R. Bank, *Fellow, IEEE*, Avik W. Ghosh, *Senior Member, IEEE*, and Joe C. Campbell, *Life Fellow, IEEE*

***Abstract*—Digital alloy $Al_{0.85}Ga_{0.15}As_{0.56}Sb_{0.44}$, random alloy $Al_{0.85}Ga_{0.15}As_{0.56}Sb_{0.44}$, and random alloy $Al_{0.79}In_{0.21}As_{0.74}Sb_{0.26}$ are promising candidates for the multiplication regions of avalanche photodiodes (APDs) due to their low excess noise, which is comparable to that of Si APDs. The temperature dependence of avalanche breakdown in these materials has been investigated by measuring the multiplication gain. A weak temperature dependence of the breakdown voltage is observed, which is desirable to reduce the complexity of temperature or reverse bias control circuits in the optical receiver. Calculations of the alloy disorder potentials and alloy scattering rates indicate that the temperature dependence of the avalanche breakdown in these quaternary alloys is attributable to the dominance of large mass variations and high alloy scattering over phonon scattering. Impact ionization can also be impacted by the temperature dependence of the bandgap energy which affects the ionization threshold energy. Therefore, the temperature dependence of the bandgap energy has been investigated by temperature-dependent photoluminescence and external quantum efficiency measurements to further explain the temperature dependent breakdown characteristics of these materials.**

***Index Terms*—AlGaAsSb, AlInAsSb temperature dependence, avalanche breakdown, bandgap energy, digital alloy, random alloy.**

Manuscript received 8 March 2022; revised 11 May 2022 and 17 June 2022; accepted 20 June 2022. Date of publication 22 June 2022; date of current version 2 September 2022. This work was supported in part by Directed Energy–Joint Technology Office (DE-JTO) under Grant N00014-17-1-2440, in part by the Army Research Office and DARPA under Grant W911NF-17-1-0065, in part by DARPA under Grant W909MY-12-D-0008, and in part by the National Science Foundation under Grant NSF1936016. *(Corresponding author: Joe C. Campbell.)*

Bingtian Guo, Sheikh Z. Ahmed, Xingjun Xue, Andrew H. Jones, Avik W. Ghosh, and Joe C. Campbell are with the Department of Electrical and Computer Engineering, University of Virginia, Charlottesville, VA 22904 USA (e-mail: bg8ws@virginia.edu; sza9wz@virginia.edu; xingjunxue@gmail.com; ahj2ge@virginia.edu; ag7rq@virginia.edu; jcc7s@virginia.edu).

Ann-Kathryn Rockwell, J. Andrew McArthur, and Seth R. Bank are with the Department of Electrical and Computer Engineering, University of Texas, Austin, TX 78758 USA (e-mail: akrockwell@utexas.edu; jandrewmcarthur@utexas.edu; sbank@ece.utexas.edu).

Jaedu Ha and Jong Su Kim are with the Department of Physics, Yeungnam University, Gyeongsan 38541, South Korea (e-mail: nopain21@ynu.ac.kr; jongsukim@ynu.ac.kr).

Seunghyun Lee, Sri H. Kodati, Theodore J. Ronningen, and Sanjay Krishna are with the Department of Electrical and Computer Engineering, The Ohio State University, Columbus, OH 43210 USA (e-mail: lee.8014@buckeyemail.osu.edu; kodati.2@buckeyemail.osu.edu; ronningen.1@osu.edu; krishna.53@osu.edu).

Baolai Liang is with the California NanoSystems Institute, University of California, Los Angeles, CA 90095 USA (e-mail: bliang@cnsi.ucla.edu).

Color versions of one or more figures in this article are available at https://doi.org/10.1109/JLT.2022.3185417.

Digital Object Identifier 10.1109/JLT.2022.3185417

I. Introduction

AVALANCHE photodiodes (APDs) are beneficial for detecting weak optical signals, leading to their utilization in a wide range of commercial, research, and military applications [1], [2]. Their internal multiplication gain results from the stochastic impact ionization process, and higher receiver sensitivity can be achieved relative to unity-gain photodiodes. Typically, in the impact ionization process, the carriers obtain the ionization threshold energy by accelerating in a high electric field multiplication region [3], and loss of energy occurs primarily through scattering, with phonon scattering being dominant. Phonon scattering exhibits strong positive temperature dependence. This results in significant variation of the gain with temperature; higher reverse bias is required to maintain the same gain at higher temperature. In practice, in order to maintain a stable gain, an active variable bias circuit or a thermoelectric cooler is required to control either the applied reverse bias or the operating temperature, increasing the cost and the system complexity [4]. The simplest and most straightforward way to simplify the bias or temperature control circuits is to choose a multiplication material with weak temperature dependence of avalanche breakdown. The temperature sensitivity is characterized by the temperature coefficient of breakdown voltage [5], which is expressed as

$$C_{bd} = \frac{\Delta V_{bd}}{\Delta T}, \tag{1}$$

where ΔV_{bd} is the change of the breakdown voltage, and ΔT is the change of the temperature. The temperature coefficient of breakdown voltage is determined by not only the material but also the multiplication layer thickness. As the multiplication layer thickness increases, C_{bd} increases due to increased phonon scattering [6].

The choice of the multiplication layer material is determined by various factors including dark current, excess noise, and the temperature coefficient of the breakdown voltage. The excess noise is typically included as a multiplicative term, referred to as the excess noise factor, *F(M),* in the shot noise current, i_{shot}, which can be expressed as [7]

$$\left\langle i_{shot}^2 \right\rangle = 2q\left(I_{photo} + I_{dark}\right) M^2 F\left(M\right) \Delta f, \tag{2}$$

where I_{photo} and I_{dark} are the photocurrent and dark current, respectively, M is the average value of the gain, and Δf is the

bandwidth. In the local field model for pure electron injection [7],

$$F(M) = kM + (1-k)\left(2 - \frac{1}{M}\right), \tag{3}$$

where k is the ratio of the hole impact ionization coefficient to the electron impact ionization coefficient. A lower k value is desirable to reduce the excess noise, leading to higher receiver sensitivity and higher gain-bandwidth product. Recently, $Al_xIn_{1-x}As_ySb_{1-y}$ and $Al_xGa_{1-x}As_ySb_{1-y}$ material systems [2] have been reported k values comparable to that of Si ($k \sim 0.01$) [7], [8] and lower than that of $In_{0.52}Al_{0.48}As$ ($k \sim 0.2$) [9], [10] or InP ($k \sim 0.45$) [11]. These two Sb-based material systems are promising candidates for the multiplication regions in the separate absorption, charge, and multiplication (SACM) APDs. Furthermore, thick digital alloy (DA) $Al_xIn_{1-x}As_ySb_{1-y}$ lattice-matched to GaSb with x = 0.6, 0.7, 0.8, [12]–[14] and thin random alloy (RA) $Al_xGa_{1-x}As_{0.56}Sb_{0.44}$ lattice-matched to InP with x = 1, 0.95, 0.9, 0.85 [15], [16] have shown a weak temperature dependence of avalanche breakdown. Recently, we have reported low k values for thick random alloy $Al_{0.79}In_{0.21}As_{0.74}Sb_{0.26}$ APDs [17], thick digital alloy $Al_{0.85}Ga_{0.15}As_{0.56}Sb_{0.44}$ APDs [18], and thick random alloy $Al_{0.85}Ga_{0.15}As_{0.56}Sb_{0.44}$ [19] APDs lattice-matched to InP. It follows that it is useful to determine the temperature characteristics of these material systems.

In this work, the avalanche breakdown with temperature variation was studied for digital alloy $Al_{0.85}Ga_{0.15}As_{0.56}Sb_{0.44}$, random alloy $Al_{0.85}Ga_{0.15}As_{0.56}Sb_{0.44}$ (hereafter $Al_{0.85}$GaAsSb), and random alloy $Al_{0.79}In_{0.21}As_{0.74}Sb_{0.26}$ (hereafter $Al_{0.79}$InAsSb) p^+-i-n^+ APDs. An explanation for the weak temperature dependence of avalanche breakdown is provided by calculating alloy disorder potentials and alloy scattering rates. In addition, the variation of the bandgap with temperature was investigated with photoluminescence and quantum efficiency measurements.

II. Epitaxial Crystal Growth and Device Fabrication

All three wafers were grown as p^+-i-n^+ structures by molecular beam epitaxy. One of the $Al_{0.85}$GaAsSb wafers lattice-matched to InP was grown as a digital alloy [18] and the other as a random alloy [19]. The $Al_{0.79}$InAsSb wafer lattice-matched to InP was grown as a random alloy [17]. The layer structures are shown in Table I, and the multiplication layer thickness were taken from capacitance-voltage (C-V) measurements [20]. Be and Si were used as p-type and n-type dopants, respectively.

Circular mesa structures were defined by photolithography and formed by the chemical etching with a solution of citric and phosphoric acid [21]. The top and bottom Ti and Au contacts were then deposited by electron-beam evaporation. Finally, the sidewalls were passivated by SU-8 to suppress the surface dark current.

TABLE I
Epitaxial Structures of p^+-i-n^+ APDs

Types	Material	Thickness (nm)	Doping (cm^{-3})
Digital alloy $Al_{0.85}$GaAsSb p^+-i-n^+ APD	InGaAs	20	p^{++}: 1×10^{19}
	$Al_{0.85}$GaAsSb	300	p^+: 2×10^{18}
	$Al_{0.85}$GaAsSb	890	UID
	$Al_{0.85}$GaAsSb	100	n^+: 2×10^{18}
	InGaAs	400	n^{++}: 1×10^{19}
	Semi-insulating InP substrate		
Random alloy $Al_{0.85}$GaAsSb p^+-i-n^+ APD	InGaAs	20	p^{++}: 1×10^{19}
	$Al_{0.85}$GaAsSb	300	p^+: 2×10^{18}
	$Al_{0.85}$GaAsSb	1020	UID
	$Al_{0.85}$GaAsSb	100	n^+: 2×10^{18}
	InGaAs	500	n^{++}: 1×10^{19}
	Semi-insulating InP substrate		
Random alloy $Al_{0.79}$InAsSb p^+-i-n^+ APD	InGaAs	20	p^{++}: 1×10^{19}
	$Al_{0.79}$InAsSb	300	p^+: 2×10^{18}
	$Al_{0.79}$InAsSb	1100	UID
	$Al_{0.79}$InAsSb	100	n^+: 2×10^{18}
	InGaAs	500	n^{++}: 1×10^{19}
	Semi-insulating InP substrate		

III. Temperature-Dependent Avalanche Breakdown

APDs were placed in a nitrogen-cooled cryogenic chamber, and a temperature controller was used to monitor the temperature. The current-voltage (I-V) characteristics of 150-um-diameter APDs were measured under dark and illuminated conditions. A 520-nm fiber-coupled laser source was used to illuminate the device. The gain, M, was calculated from the photocurrent, and the breakdown voltage can be determined by the extrapolation of the inverse gain, $1/M$, to zero. This $1/M$ extrapolation method has been utilized in various $Al_xGa_{1-x}As_ySb_{1-y}$ and $Al_xIn_{1-x}As_ySb_{1-y}$ samples, and a good linear fitting of $1/M$ data has been obtained [12]–[16]. Due to the absence of temperature-dependent impact ionization coefficients for $Al_{0.85}$GaAsSb and $Al_{0.79}$InAsSb, the breakdown voltage cannot be directly determined by the simulation of multiplication gain for these three samples [4]. Finally, the temperature coefficient of breakdown voltage, C_{bd}, is the slope of the linear fitting to the breakdown voltages under different temperatures.

Fig. 1 shows (a) the gain versus voltage, (b) the inverse gain curves, and (c) the dark current in the range of 78 K to 360 K for DA $Al_{0.85}$GaAsSb APDs. Fig. 2 shows similar curves for RA $Al_{0.85}$GaAsSb APDs in the temperature range of 200 K to 340 K. The measurements on RA $Al_{0.79}$InAsSb APDs in the temperature range of 200 K to 320 K are shown in Fig. 3. Based on the linear regression approach, the fitting curves of breakdown voltages under different temperatures are calculated in Fig. 4, and the C_{bd} is determined to be (4.22 ± 0.08) mV/K, (5.92 ± 0.36) mV/K, and (5.91 ± 0.37) mV/K for DA $Al_{0.85}$GaAsSb, RA $Al_{0.85}$GaAsSb, and RA $Al_{0.79}$InAsSb APDs. Values of C_{bd} for these three materials, commercially available materials (including InP, InAlAs, Si [5], [6]), and recently reported Sb-based materials [4], [12]–[16] are shown in Fig. 5. The temperature coefficient of breakdown voltage of these three materials are significantly lower than InP, InAlAs, or Si [5], [6] with the same multiplication layer thickness.

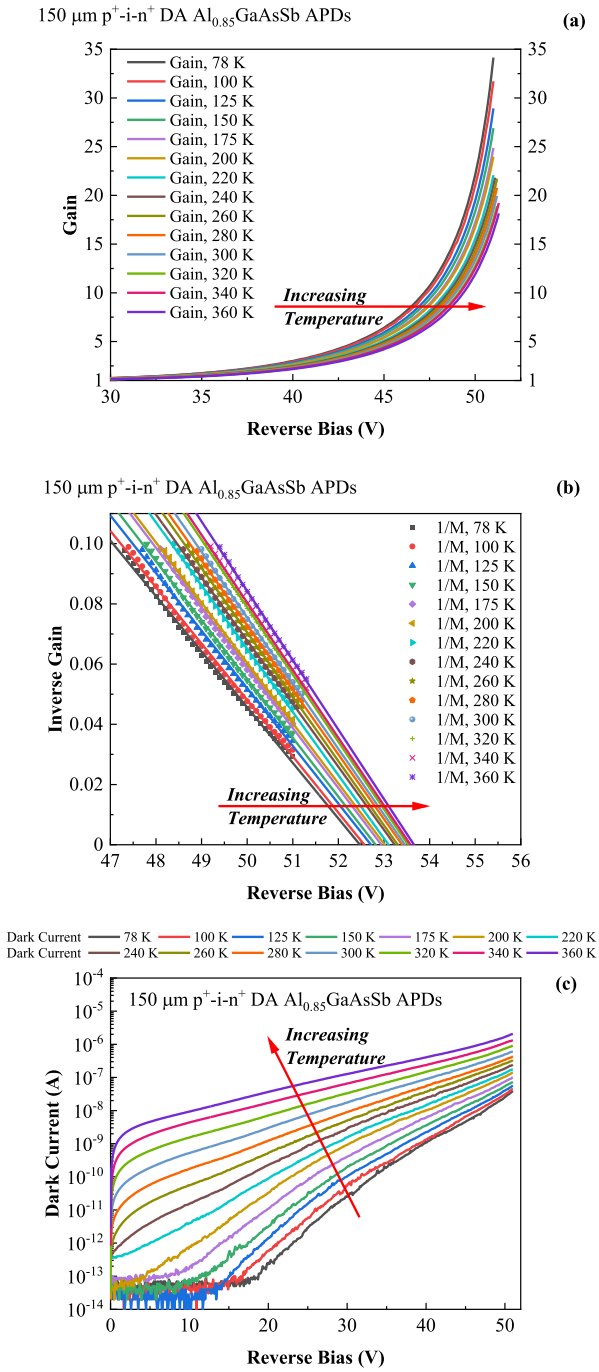

Fig. 1. (a) Measured gain curves, (b) Inverse gain (symbols) and linear fitting (solid lines) under 520-nm illumination, and (c) Dark current curves for 150-μm-diameter p$^+$-i-n$^+$ DA $Al_{0.85}GaAsSb$ APDs from 78 K to 360 K.

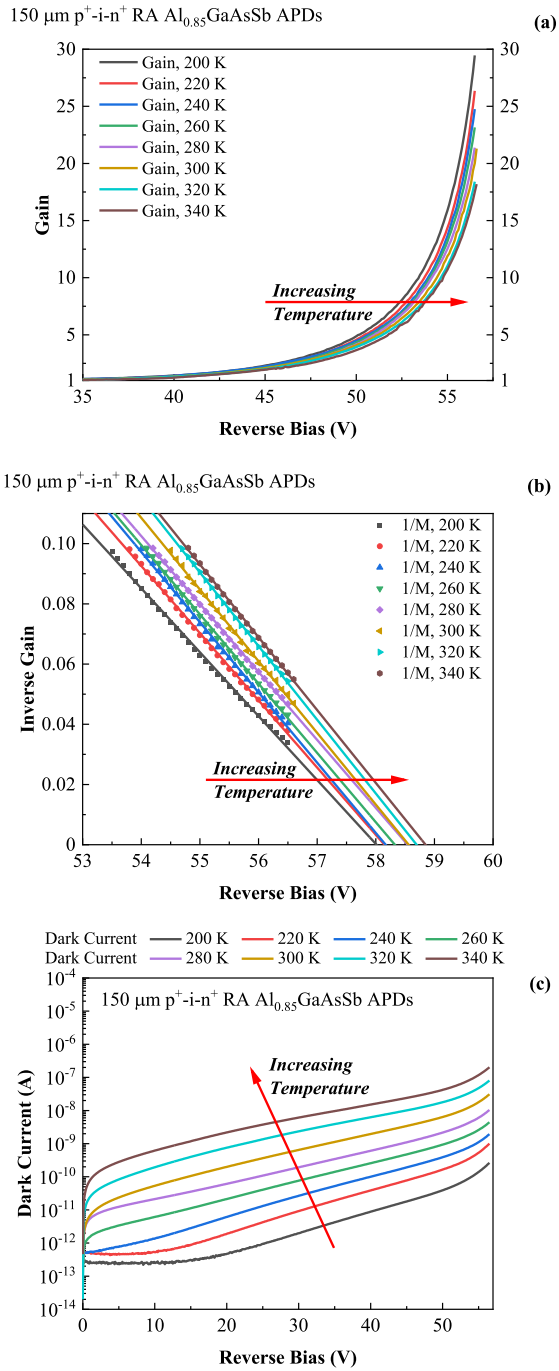

Fig. 2. (a) Measured gain curves, (b) Inverse gain (symbols) and linear fitting (solid lines) under 520-nm illumination, and (c) Dark current curves for 150-μm-diameter p$^+$-i-n$^+$ RA $Al_{0.85}GaAsSb$ APDs from 200 K to 340 K.

IV. Discussion

A. Role of Alloy Scattering in Sb-Based Quaternary Alloys

Previously, it has been observed that ternary alloys have lower C_{bd} compared to binary compounds [22]. The low C_{bd} of ternary alloys was attributed to the dominance of alloy scattering over phonon scattering. In a random alloy, for example a ternary alloy, the constituent atoms are distributed in a random manner which leads to fluctuations in the crystal potential. This fluctuating potential results in an effective scattering process, referred to as alloy scattering, which impacts the movement of electrons through the crystal [23]. In contrast, the digital alloys are short-period superlattices that consist of binary alloy layers stacked alternately in a periodic manner. Due to the small thickness of these binary layers, there is interface roughness, leading to fluctuations of the crystal potential at the interfaces. This paper has demonstrated that Sb-based quaternary alloys exhibit even lower C_{bd} in comparison to both ternary and binary alloys.

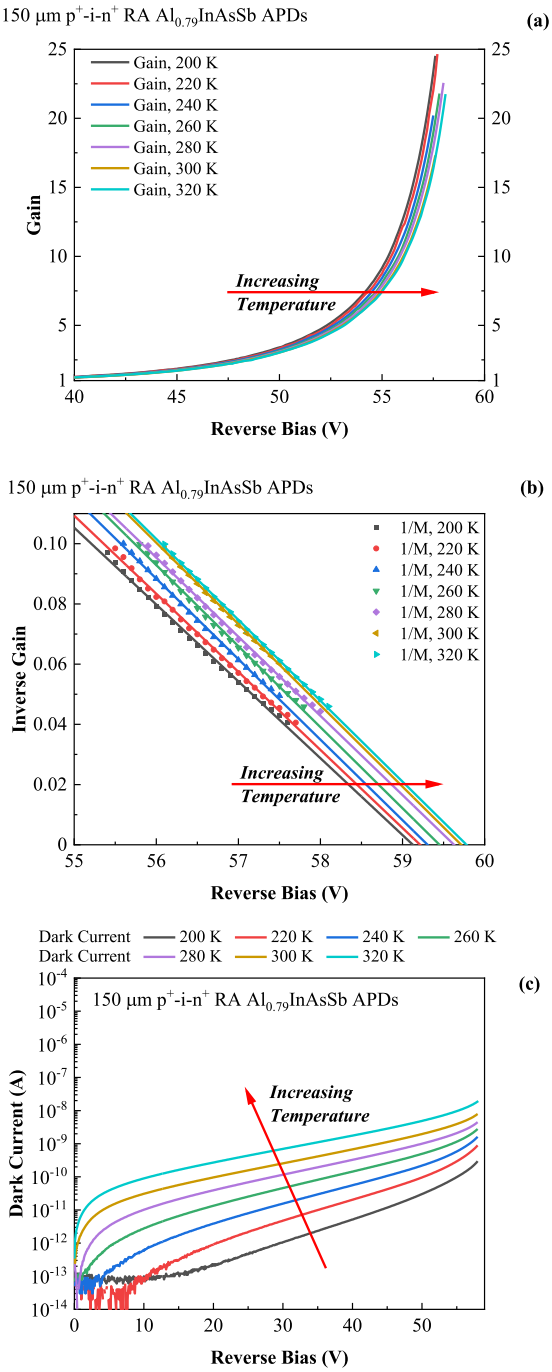

Fig. 3. (a) Measured gain curves, (b) Inverse gain (symbols) and linear fitting (solid lines) under 520-nm illumination, and (c) Dark current curves for 150-μm-diameter p^+-i-n^+ RA $Al_{0.79}InAsSb$ APDs from 200 K to 320 K.

Thus, it appears that alloy scattering also plays a significant role in the temperature dependence of the breakdown voltage for these materials. To understand the significance of this scattering mechanism in these materials, their alloy disorder potentials and alloy scattering rates were studied.

The alloy scattering rate for a quaternary alloy is given by [24]

$$\frac{1}{\tau} = \frac{3\pi}{8\sqrt{2}} \frac{(m^*)^{3/2}}{\hbar^4} \gamma(E) \frac{d\gamma}{dE} \Omega |\Delta U_Q(x,y)|^2 S \qquad (4)$$

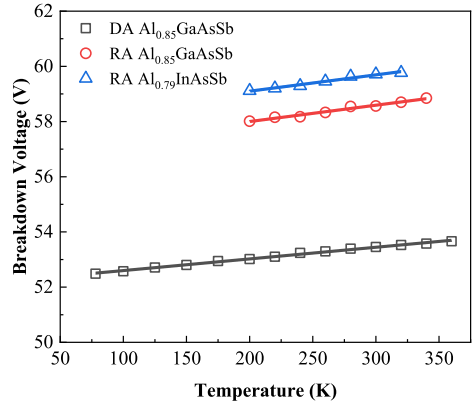

Fig. 4. Temperature dependence of avalanche breakdown for p^+-i-n^+ DA $Al_{0.85}GaAsSb$, RA $Al_{0.85}GaAsSb$, and RA $Al_{0.79}InAsSb$ APDs. Symbols are measured breakdown voltages, and solid lines are linear fitting curves.

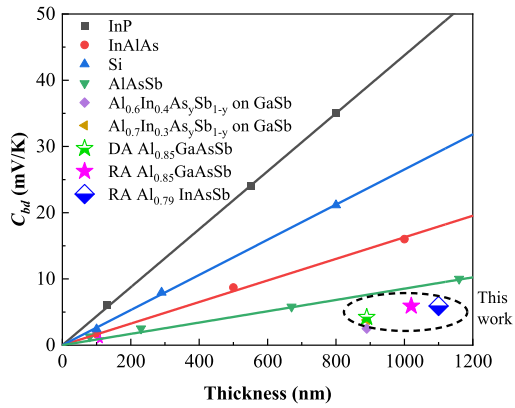

Fig. 5. Comparison of the temperature coefficient of breakdown voltage between studied DA $Al_{0.85}GaAsSb$ (green star), RA $Al_{0.85}GaAsSb$ (pink star), RA $Al_{0.79}InAsSb$ (blue square), and other materials including InP [5], InAlAs [5], Si [6], AlAsSb [4], thin RA $Al_{0.85}GaAsSb$ lattice-matched to InP [16], and thick DA AlxIn1-xAsySb1-y lattice-matched to GaSb with x = 0.6, 0.7 [12]. Symbols are measured values, and solid lines are linear fits.

with

$$|\Delta U_Q(x,y)|^2 = x(1-x)y^2|\Delta U_{ABD}|^2 + x(1-x)(1-y)^2 \times |\Delta U_{ABC}|^2 + x^2 y(1-y)|\Delta U_{BCD}|^2 + (1-x)^2 y(1-y)|\Delta U_{ACD}|^2,$$

where the ΔU_Q is the alloy disorder potential of the quaternary alloy. The ΔU's on the right hand side of the equation represent the disorder potential of ternary alloys. For example, the potential ΔU_{ABD} is for a ternary alloy with composition $A_{1-x}B_xD$, and the potential ΔU_{BCD} is for $BC_{1-y}D_y$. The alloy disorder potential arises due to the potential fluctuations created by the different nuclei sizes of the constituent atoms. In (4), m^* is the carrier effective mass, Ω is the primitive cell volume, and $\gamma(E) = E(1+\sigma E)$ describes the non-parabolic nature of the electronic band structure with E representing the carrier energy and σ describing the non-parabolicity. The ordering of atoms is described by the factor S. For completely random systems $S = 1$, and $S = 0$ for perfectly ordered systems. In our simulations, we assume $S = 1$. For a ternary alloy $A_{1-x}B_xC$, the disorder potential

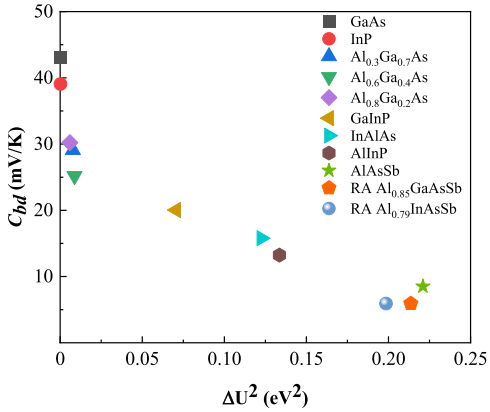

Fig. 6. Comparison of C_{bd} vs. ΔU^2 for various III-V binary, ternary, and quaternary alloys.

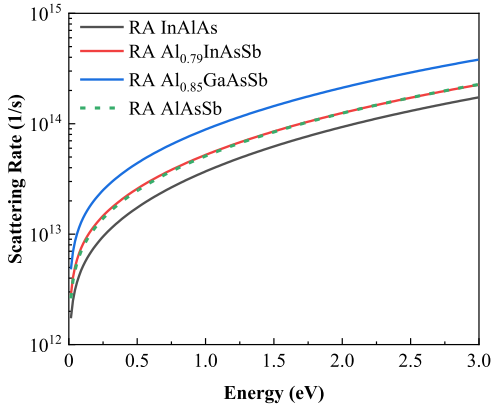

Fig. 7. Comparison of scattering rates for random alloys of InAlAs, $Al_{0.79}InAsSb$, $Al_{0.85}GaAsSb$, and AlAsSb.

can be calculated by

$$\Delta U = \frac{bZ}{4\pi\varepsilon_0}\left(\frac{1}{r_A}-\frac{1}{r_B}\right)\exp\left(-k_s R\right), \tag{5}$$

where b accounts for the fact that the Thomas Fermi theory overestimates the screening in the semiconductor and has a value of 1.5 for most zinc blende binary semiconductors. Z is the valence number of A and B, ε_0 is the vacuum permittivity, and the covalent radii of the atoms A, B and C are given by r_A, r_B, and r_C, respectively.$k_s = \sqrt{4k_F/\pi a_B}$is the Thomas Fermi screening wave number in a three-dimensional system, where a_B is the Bohr radius, and $k_F = (3\pi^2 N_{val})^{1/3}$ is the Fermi wave number in a three-dimensional system. The valence electron density $N_{val} = 32/a^3$, and the bond length of this ternary alloy $R = 0.5[xr_A + (1-x)r_B + r_C]$.

In (5), it is seen that the alloy disorder potential primarily depends on the difference in covalent radii of the constituent atoms and their valence number. Fig. 6 shows the comparison of C_{bd} vs. ΔU^2 for various III-V binary, ternary, and quaternary alloys. The ternary alloy potentials are scaled by the factor x(1-x), where x is the mole fraction for atom B in AB_xC_{1-x}, to make a valid comparison with quaternary alloy potentials [22]. The C_{bd} values for the binary and ternary alloys are obtained from the literature [4], [22], and they are for the APDs with 1-μm multiplication layer thickness. A larger radii difference leads to a higher alloy disorder potential. For example, InAlAs has a larger potential in comparison to AlGaAs because there is a large difference in the Al and In covalent radii whereas the Al and Ga covalent radii are similar. Also, alloys with different group V elements have a higher disorder potential in comparison to alloys with varying group III elements due to the larger valence number of group V elements.

We computed the alloy disorder potentials for the Sb-based quaternary alloys by using (5). $\Delta U = 0.46$ eV for RA $Al_{0.85}GaAsSb$ and $\Delta U = 0.45$ eV for RA $Al_{0.79}InAsSb$ were obtained. The ΔU^2 of the Sb-based ternary and quaternary alloys are significantly larger than other III-V alloys shown in Fig. 6. Consequently, the breakdown voltage of the Sb-based alloys has the weakest temperature dependence due to the large difference in the covalent radii of As and Sb atoms, which are also group V elements. The resulting higher disorder potential of these alloys leads to an increased alloy scattering rate, given by (4), which then dominates over the phonon scattering leading to a weaker temperature dependence of the avalanche breakdown. The underlying factor for the temperature dependence of the avalanche breakdown is phonon scattering which can be altered by the temperature-dependent phonon population. A more dominant scattering mechanism, like alloy scattering, suppresses the phonon scattering mechanism which ultimately reduces the temperature dependence.

To further highlight the role of Sb atoms in the quaternary alloys, we plotted the alloy scattering rates of RA InAlAs, RA $Al_{0.79}InAsSb$, RA $Al_{0.85}GaAsSb$ and RA AlAsSb in Fig. 7. The quaternary alloys containing Sb demonstrate much higher scattering rates in comparison to that of the ternary InAlAs. The higher scattering rates of the quaternary alloys arise from their higher alloy disorder potentials, and potentially lower electron-phonon coupling. This is consistent with experimental observation that InAlAs has a stronger temperature dependence of avalanche breakdown than the quaternary alloys do. In the simulation, we used effective masses of $0.072m_0$, $0.11m_0$, $0.15m_0$, and $0.098m_0$ for InAlAs, $Al_{0.79}InAsSb$, $Al_{0.85}GaAsSb$, and AlAsSb, respectively. The corresponding bandgaps for these four materials are 1.4 eV, 1.73 eV, 1.59 eV and 1.65 eV. The lattice constant of InP (5.9117 Å), which is the substrate for all three alloys, is used. The DA scattering rates cannot be included here since their corresponding value of S is unknown. The values can be extracted by carrying out Monte Carlo simulations with alloy scattering for these alloys and calibrating with experimental results.

The origin of the weak temperature dependence of the quaternary Sb-based digital alloys can also be attributed to the dominance of the alloy scattering mechanism. In the short-period digital alloys, the edges of the thin binary layers are not completely abrupt. There is random variation in chemical composition at the interfaces which leads to interface roughness. This results in fluctuations of the crystal potential. In the Sb-based alloys, the alternating Sb and As binary alloys with large nuclei difference, create large potential fluctuations at the interface that lead to a higher disorder potential. Consequently, the resulting higher

alloy scattering rate in these quaternary digital alloys leads to their weak temperature dependence of avalanche breakdown. This mechanism potentially causes the Sb-based digital alloys to have a lower C_{bd} in comparison to random alloys, as shown in Fig. 4. This postulate can be confirmed by using Monte Carlo based simulations, which are outside the scope of this paper. In summary, phonon scattering is the dominant scattering mechanism in materials with high C_{bd}, while alloy scattering is the superior scattering mechanism in low C_{bd} materials.

B. Temperature Dependence of Bandgap Energy

The impact ionization process requires carriers to obtain the ionization threshold energy which depends on the bandgap energy, and the bandgap changes with temperature. The threshold energy determines the breakdown voltage of a material. Therefore, the temperature dependence of the material bandgap has a higher order effect on the breakdown voltage. The breakdown voltage temperature dependence is primarily due to the scattering processes, like phonon and alloy scattering, as mentioned earlier. Since the bandgap stability under different temperatures has some impact on the temperature dependence of avalanche breakdown, and it is instructive to investigate the bandgap stability of Sb-based quaternary materials as well.

Temperature-dependent photoluminescence (PL) [25] measurement was used to investigate the temperature dependence of the bandgap energy for DA $Al_{0.5}In_{0.5}As_ySb_{1-y}$ lattice-matched to GaSb [26], RA $Al_{0.79}InAsSb$ lattice-matched to InP [17], and DA $Al_{0.85}GaAsSb$ lattice-matched to InP [18]. The measured bandgap energy can be fitted by the Varshni equation [27],

$$E(T) = E_0 - \frac{\alpha T^2}{T + \beta}, \tag{6}$$

where $E(T)$ is the energy gap at temperature T, E_0 is the energy gap at 0 K, and α and β are constants.

As shown in Fig. 8(a) and (b), the bandgap of DA $Al_{0.5}In_{0.5}As_ySb_{1-y}$ and RA $Al_{0.79}InAsSb$ was determined in the temperature range of 95 K–295 K and 160 K–300 K, respectively. The data points were then fitted by the Varshni equation [27]. The temperature-dependent bandgap curves of these two Sb-based quaternary materials were compared with binary materials (including AlAs, AlSb, InAs, InSb [28]); the Sb-based materials exhibit smaller shifts with temperature. Furthermore, the results show that both digital alloy growth and random alloy growth can provide the weak temperature dependence of bandgap for $Al_xIn_{1-x}As_ySb_{1-y}$. Therefore, the digital alloy growth itself cannot explain the bandgap stability. Fig. 8(c) shows the temperature-dependent bandgap for DA $Al_{0.85}GaAsSb$ in the temperature range of 160 K to 300 K, and the data points were fitted by the Varshni equation [27]. The same conclusion that the temperature dependence of the bandgap of the quaternary material is weaker than binary materials (including AlAs, AlSb, GaAs, GaSb [28]) can be drawn for DA $Al_{0.85}GaAsSb$.

Temperature-dependent external quantum efficiency (EQE) measurement [21] was carried out to investigate spectrum cutoff

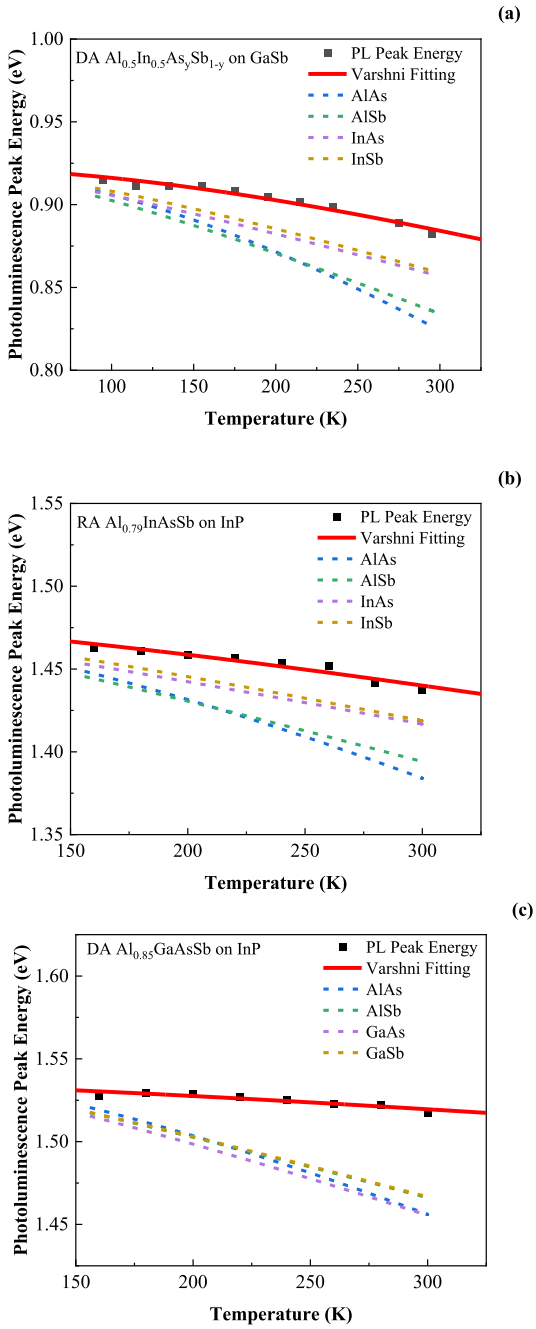

Fig. 8. Temperature-dependent photoluminescence peaks (points) and the Varshni fitting curves (solid lines) for (a) DA $Al_{0.5}In_{0.5}AsySb_{1-y}$ lattice-matched to GaSb, (b) RA $Al_{0.79}InAsSb$ lattice-matched to InP, and (c) DA $Al_{0.85}GaAsSb$ lattice-matched to InP. The dash lines represent the Varshni fitting curves for the binary materials including AlAs, AlSb, InAs, InSb, GaAs, GaSb [28], and the E0 of binary materials has been modified accordingly for a better comparison with the investigated quaternary materials.

under different temperatures for DA $Al_{0.7}In_{0.3}As_ySb_{1-y}$ lattice-matched to GaSb [29]. As shown in Fig. 9, external quantum efficiency measurements were carried out in the temperature range of 258.15 K to 298.15 K for DA $Al_{0.7}In_{0.3}As_ySb_{1-y}$. Based on shifts in the response near cutoff, the bandgap variation with temperature was determined to be 0.29 meV/K, which is consistent with the PL measurements. In summary, both

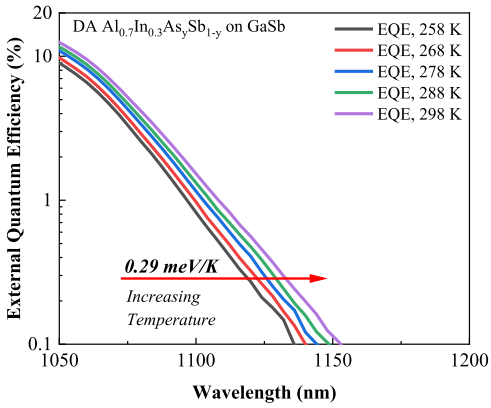

Fig. 9. Temperature-dependent external quantum efficiency for DA $Al_{0.7}In_{0.3}AsySb_{1-y}$ lattice-matched to GaSb.

temperature-dependent PL measurements and EQE measurements demonstrate weak variation of the bandgap with temperature for $Al_xIn_{1-x}As_ySb_{1-y}$ and $Al_xGa_{1-x}As_ySb_{1-y}$ material systems, irrespective of growth method. The temperature dependence of the material bandgap is primarily attributed to electron-phonon interactions [30] that broaden the material energy states and result in the creation of energy states within the bandgap. The effect of thermal expansion on the temperature dependence is very small for covalent compounds [31]. The weak temperature dependence of bandgap for these Sb-based quaternary alloys most likely arises from the weak electron-phonon coupling in these materials. The weak coupling results in a small broadening of the energy states and hence fewer energy levels created within the bandgap. It is possible that such weak temperature dependence of the material bandgap will somewhat lower the C_{bd} primarily as a higher order effect. On the other hand, a stronger electron-phonon coupling will most likely cause some increase in C_{bd}. Further investigations are needed to be carried out to determine the exact contribution of electron-phonon interactions on C_{bd}.

V. Conclusion

Temperature dependence of avalanche breakdown has been investigated for digital alloy $Al_{0.85}Ga_{0.15}As_{0.56}Sb_{0.44}$, random alloy $Al_{0.85}Ga_{0.15}As_{0.56}Sb_{0.44}$, and random alloy $Al_{0.79}In_{0.21}As_{0.74}Sb_{0.26}$. We observe weak dependence of the avalanche breakdown voltage on temperature for the Sb-based quaternary materials. Temperature-dependent photoluminescence and external quantum efficiency measurements reveal weak temperature dependence of the bandgap. Modeling supports that these quaternary alloys have high alloy scattering rates dominating over phonon scattering mechanisms that reduce the temperature dependence of the avalanche breakdown. This weak temperature dependence has the benefit of simplifying the temperature or reverse bias control circuits while maintaining a constant multiplication gain in an optical receiver.

References

[1] J. C. Campbell, "Recent advances in avalanche photodiodes," *J. Lightw. Technol.*, vol. 34, no. 2, pp. 278–285, 2016.
[2] J. C. Campbell, "Evolution of low-noise avalanche photodetectors," *IEEE J. Sel. Topics Quantum Electron.*, vol. 28, no. 2, Mar./Apr. 2022, Art. no. 3800911.
[3] K. Yeom, J. M. Hinckley, and J. Singh, "Theoretical study on threshold energy and impact ionization coefficient for electrons in $Si_{1-x}Ge_x$," *Appl. Phys. Lett.*, vol. 64, no. 22, pp. 2985–2987, 1994.
[4] X. Jin et al., "Temperature dependence of the impact ionization coefficients in AlAsSb lattice matched to InP," *IEEE J. Sel. Topics Quantum Electron.*, vol. 28, no. 2, Mar./Apr. 2022, Art. no. 3801208.
[5] L. J. J. Tan et al., "Temperature dependence of avalanche breakdown in InP and InAlAs," *IEEE J. Quantum Electron.*, vol. 46, no. 8, pp. 1153–1157, Aug. 2010.
[6] D. J. Massey, J. P. R. David, and G. J. Rees, "Temperature dependence of impact ionization in submicrometer silicon devices," *IEEE Trans. Electron. Devices*, vol. 53, no. 9, pp. 2328–2334, Sep. 2006.
[7] C. A. Lee, R. A. Logan, R. L. Batdorf, J. J. Kleimack, and W. Wiegmann, "Ionization rates of holes and electrons in silicon," *Phys. Rev.*, vol. 134, no. 3A, 1964, Art. no. A761.
[8] V. M. Robbins, T. Wang, K. F. Brennan, K. Hess, and G. E. Stillman, "Electron and hole impact ionization coefficients in (100) and in (111) Si," *J. Appl. Phys.*, vol. 58, no. 12, pp. 4614–4617, 1985.
[9] C. Lenox et al., "Thin multiplication region InAlAs homojunction avalanche photodiodes," *Appl. Phys. Lett.*, vol. 73, no. 6, pp. 783–784, 1998.
[10] Y. L. Goh et al., "Excess avalanche noise in $In_{0.52}Al_{0.48}As$," *IEEE J. Quantum Electron.*, vol. 43, no. 5/6, pp. 503–507, 2007.
[11] L. J. J. Tan, J. S. Ng, C. H. Tan, and J. P. R. David, "Avalanche noise characteristics in submicron InP diodes," *IEEE J. Quantum Electron.*, vol. 44, no. 4, pp. 378–382, Apr. 2008.
[12] A. H. Jones, Y. Yuan, M. Ren, S. J. Maddox, S. R. Bank, and J. C. Campbell, "$Al_xIn_{1-x}As_ySb_{1-y}$ photodiodes with low avalanche breakdown temperature dependence," *Opt. Exp.*, vol. 25, no. 20, pp. 24340–24345, 2017.
[13] A. H. Jones, A. Rockwell, S. D. March, Y. Yuan, S. R. Bank, and J. C. Campbell, "High gain, low dark current $Al_{0.8}In_{0.2}As_{0.23}Sb_{0.77}$ avalanche photodiodes," *IEEE Photon. Technol. Lett.*, vol. 31, no. 24, pp. 1948–1951, Dec. 2019.
[14] Y. Yuan et al., "Comparison of different period digital alloy $Al_{0.7}$ InAsSb avalanche photodiodes," *J. Lightw. Technol.*, vol. 37, no. 14, pp. 3647–3654, 2019.
[15] S. Abdullah, C. H. Tan, X. Zhou, S. Zhang, L. Pinel, and J. S. Ng, "Investigation of temperature and temporal stability of AlGaAsSb avalanche photodiodes," *Opt. Exp.*, vol. 25, no. 26, pp. 33610–33616, 2017.
[16] X. Zhou et al., "Thin $Al_{1-x}Ga_xAs_{0.56}Sb_{0.44}$ diodes with extremely weak temperature dependence of avalanche breakdown," *Roy. Soc. Open Sci.*, vol. 4, no. 5, 2017, Art. no. 170071.
[17] S. H. Kodati et al., "AlInAsSb avalanche photodiodes on InP substrates," *Appl. Phys. Lett.*, vol. 118, no. 9, 2021, Art. no. 091101.
[18] S. Lee et al., "Low noise $Al_{0.85}Ga_{0.15}As_{0.56}Sb_{0.44}$ avalanche photodiodes on InP substrates," *Appl. Phys. Lett.*, vol. 118, no. 8, 2021, Art. no. 081106.
[19] S. Lee et al., "Random alloy thick AlGaAsSb avalanche photodiodes on InP substrates," *Appl. Phys. Lett.*, vol. 120, no. 7, 2022, Art. no. 071101.
[20] B. Guo et al., "Impact ionization coefficients of digital alloy and random alloy $Al_{0.85}Ga_{0.15}As_{0.56}Sb_{0.44}$ in a wide electric field range," *J. Lightw. Technol.*, to be published.
[21] B. Guo et al., "Optical constants of $Al_{0.85}Ga_{0.15}As_{0.56}Sb_{0.44}$ and $Al_{0.79}In_{0.21}As_{0.74}Sb_{0.26}$," *Appl. Phys. Lett.*, vol. 119, no. 17, 2021, Art. no. 171109.
[22] J. S. L. Ong, J. S. Ng, A. B. Krysa, and J. P. R. David, "Temperature dependence of avalanche multiplication and breakdown voltage in $Al_{0.52}In_{0.48}P$," *J. Appl. Phys.*, vol. 115, no. 6, Feb. 2014, Art. no. 064507.
[23] J. W. Harrison and J. R. Hauser, "Alloy scattering in ternary III-V compounds," *Phys. Rev. B*, vol. 13, no. 12, 1976, Art. no. 5347.
[24] M. A. Littlejohn, J. R. Hauser, T. H. Glisson, D. K. Ferry, and J. W. Harrison, "Alloy scattering and high field transport in ternary and quaternary III–V semiconductors," *Solid-State Electron.*, vol. 21, no. 1, pp. 107–114, 1978, doi: 10.1016/0038-1101(78)90123-5.
[25] S. Lee et al., "Investigation of carrier localization in InAs/AlSb type-II superlattice material system," *Appl. Phys. Lett.*, vol. 115, no. 21, 2019, Art. no. 211601.
[26] M. Ren, S. J. Maddox, M. E. Woodson, Y. Chen, S. R. Bank, and J. C. Campbell, "Characteristics of $Al_xIn_{1-x}As_ySb_{1-y}$ (x: 0.3∼0.7) avalanche photodiodes," *J. Lightw. Technol.*, vol. 35, no. 12, pp. 2380–2384, 2017.
[27] Y. P. Varshni, "Temperature dependence of the energy gap in semiconductors," *Physica*, vol. 34, no. 1, pp. 149–154, 1967.

[28] I. Vurgaftman, J. R. Meyer, and L. R. Ram-Mohan, "Band parameters for III–V compound semiconductors and their alloys," *J. Appl. Phys.*, vol. 89, no. 11, pp. 5815–5875, 2001.
[29] M. E. Woodson, M. Ren, S. J. Maddox, Y. Chen, S. R. Bank, and J. C. Campbell, "Low-noise AlInAsSb avalanche photodiode," *Appl. Phys. Lett.*, vol. 108, no. 8, 2016, Art. no. 081102.
[30] M. Cardona and M. L. W. Thewalt, "Isotope effects on the optical spectra of semiconductors," *Rev. Modern Phys.*, vol. 77, no. 4, 2005, Art. no. 1173.
[31] Y. Zhang, Z. Wang, J. Xi, and J. Yang, "Temperature-dependent band gaps in several semiconductors: From the role of electron–phonon renormalization," *J. Phys.: Condens. Matter*, vol. 32, no. 47, 2020, Art. no. 475503.

Bingtian Guo received the B.S. degree in opto-electronics information science and engineering from Nankai University, Tianjin, China, in 2019. He is currently working toward the Ph.D. degree in electrical engineering with the University of Virginia, Charlottesville, VA, USA. His research interests include high-power and high-speed photodiodes.

Sheikh Z. Ahmed received the B.Sc. degree from BRAC University, Dhaka, Bangladesh, and the Ph.D. degree from the University of Virginia, Charlottesville, VA, USA. He is currently with Intel Corporation. His research interests include the computational study of nanoelectronic and photonic devices, analytical modeling, quantum transport, and compact modeling.

Xingjun Xue received the B.E. degree in electronic and information engineering from Xidian University, Xi'an, China, in 2013, and the Ph.D. degree in electronic science and technology from Tsinghua University, Beijing, China, in 2019. She is currently a Research Associate with the Department of Electrical and Computer Engineering, University of Virginia, Charlottesville, VA, USA. Her research interests include the design, fabrication, and characterization of avalanche photodiode.

Ann-Kathryn Rockwell received the B.S. degree from the University of Alabama, Tuscaloosa, AL, USA, in 2013, and the M.S. degree in electrical engineering in 2016 from the University of Texas at Austin, Austin, TX, USA, where she is currently working toward the Ph.D. degree in electrical engineering. Her current research interests include the design, MBE growth, and characterization of III-V materials for use in low-noise avalanche photodiodes.

Jaedu Ha received the M.Sc. degree in 2016 from the Department of Physics, Yeungnam University, Gyeongsan, South Korea, where he is currently working toward the Ph.D. degree. His current research focuses on the semiconductor material characterization for optoelectronics applications. His main research focuses on measurement and analysis of emerging materials using various spectroscopy techniques.

Seunghyun Lee received the M.Eng. degree in 2021 from The Ohio State University, Columbus, OH, USA, where he is currently working toward the Ph.D. degree in electrical and computer engineering. His research interests include the development of high-sensitivity and high-speed avalanche photodiodes for telecommunication networks and light detection and ranging (LiDAR) systems. His research focuses on growing extremely low-impurity materials and designing a novel device structure for various device applications.

Baolai Liang received the Ph.D. degree in microelectronics-photonics from the University of Arkansas, Fayetteville, AR, USA. He is currently the Director of Integrated Nanomaterials Laboratory, California NanoSystems Institute, University of California, Los Angeles, Los Angeles, CA, USA. His current research interests include molecular beam epitaxy growth and optical characterizations of low-dimensional III-V semiconductor materials for optoelectronics device application.

Andrew H. Jones received the B.S. degree in electrical engineering from Grove City College, Grove City, PA, USA, and the Ph.D. degree in electrical engineering with the University of Virginia, Charlottesville, VA, USA. He was a Navy Contractor for two years in Pittsburgh, PA, USA. He is currently a Postdoc with the Department of Electrical and Computer Engineering, University of Virginia. His research interests include photonic devices, specifically the design and fabrication of avalanche photodiodes for visible and infrared applications.

J. Andrew McArthur received the bachelor's degree in mechanical engineering from the University of Arkansas, Fayetteville, AR, USA. He is currently working toward the master's-Ph.D. degree with the University of Texas, Austin, TX, USA. Working with Prof. Seth Bank, his primary research focuses on the design and epitaxial growth of III-V photodiodes in the near- and mid-infrared wavelength range.

Sri H. Kodati received the master's degree from the University of Missouri-Kansas City, Kansas City, MO, USA, in 2016. He is currently working toward the Ph.D. degree with the Department of Electrical and Computer Engineering, The Ohio State University, Columbus, OH, USA. His research interests include develop low-cost and highly sensitive detectors for optical communications and light detection and ranging (LiDAR) applications, to replace commercial technologies. His research also focuses on the design, modeling, fabrication, and analysis of III-V detectors employing vertical and lateral architectures.

Theodore J. Ronningen received the Ph.D. degree in chemical physics from The Ohio State University, Columbus, OH, USA. He is currently a Research Scientist with the Department of Electrical and Computer Engineering, The Ohio State University. He was a Senior Research Scientist with Battelle, developing products and processes to improve the detection of hazardous materials for defense and security applications. He has been awarded ten patents. At Ohio State, he supports two university-wide initiatives, the NSF NeXUS Facility and the IIT Bombay-Ohio State Frontier Center. He is the Chair of the Out To Innovate Professional Society.

Sanjay Krishna (Fellow, IEEE) received the M.S. degree in electrical engineering and the Ph.D. degree in applied physics from the University of Michigan (UNM), Ann Arbor, MI, USA. He is currently the George R Smith Professor of engineering with ECE Department, The Ohio State University. He is also a Visiting Faculty with the Indian Institute of Technology Bombay, Mumbai, India. Than he joined UNM as a Tenure Track Faculty Member. He has more than 300 peer-reviewed journal articles (h-index = 59), ten issued patents and several keynote and invited talks. He was the recipient of several awards, including the Gold Medal from the Indian Institute of Technology, Madras, Cheenai, India, Defense Intelligence Agency Chief Scientist Award for Excellence, SPIE Technology Achievement Award, IEEE Aron Kressel Award, and UNM Teacher of the Year Award. He is a co-founder and the CTO of SK Infrared, a start-up involved with the use of IR imaging for defense and commercial applications. He is a Fellow of IEEE, OSA and SPIE.

Jong Su Kim received the bachelor's degree in physics and the master's and Ph.D. degrees in solid state physics from Yeungnam University, Gyeongsan, South Korea, in 1992, 1998, and 2002, respectively.Since 2009, he has been a Professor with the Department of Physics, Yeungnam University, and been studying various semiconductor photonic devices for the development of infrared photodetectors. His main research interests include MBE growth and investigating optical properties for the III-V semiconductors

Seth R. Bank (Fellow, IEEE) received the B.S. degree in electrical engineering from the University of Illinois at Urbana-Champaign (UIUC), Urbana, IL, USA, in 1999, and the M.S. and Ph.D. degrees in electrical engineering from Stanford University, Stanford, CA, USA, in 2003 and 2006, respectively. At UIUC, he studied the fabrication of InGaP–GaAs and InGaAs–InP HBTs. His Ph.D. research interests include the MBE growth, fabrication, and device physics of long-wavelength VCSELs and low-threshold edge-emitting lasers in the GaInNAs(Sb)–GaAs material system. In 2006, he was a Postdoctoral Scholar with the University of California, Santa Barbara, CA, USA, where his research centered on the growth of metal–semiconductor hetero- and nano-structures (e.g., ErAs nanoparticles in GaAs). In 2007, he joined the University of Texas at Austin, Austin, TX, USA, where he is currently an Associate Professor of electrical and computer engineering and the holder of the fifth Temple Foundation Endowed Faculty Fellowship. He has coauthored more than 175 papers and presentations in his research, which include the MBE growth of novel heterostructures and nanocomposites and their device applications. Dr. Bank was the recipient of the 2010 Young Investigator Program Award from ONR, 2010 NSF CAREER Award, 2009 Presidential Early Career Award for Scientists and Engineers (PECASE) nominated by ARO, 2009 Young Investigator Program Award from AFOSR, 2009 Young Scientist Award from the International Symposium on Compound Semiconductors, 2008 DARPA Young Faculty Award, 2008 Young Investigator Award from the North American MBE Meeting, and several best paper awards.

Avik W. Ghosh (Senior Member, IEEE) received the Ph.D. degree in physics from The Ohio State University, Columbus, OH, USA. He is currently a Professor of electrical and computer engineering and Professor of physics with the University of Virginia, Charlottesville, VA, USA. He has more than 100 refereed papers and book chapters and two upcoming books in the areas of computational nano-electronics and low power devices, specializing in materials to systems modeling (DFT2SPICE), including 2D materials, thin films for photodetectors, molecular electronics, subthermal switching, nanomagnetic materials and devices, and nanoscale heat flow. He received the Postdoctoral Fellowship in electrical engineering from Purdue University, West Lafayette, IN, USA. He is a Fellow of the Institute of Physics. He was the recipient of the IBM Faculty Award, NSF CAREER Award, Best Paper Award from the Army Research Office, Charles Brown New Faculty Teaching Award, and All-University Teaching Award.

Joe C. Campbell (Life Fellow, IEEE) received the B.S. degree in physics from The University of Texas at Austin, Austin, TX, USA, in 1969, and the M.S. and Ph.D. degrees in physics from the University of Illinois at Urbana-Champaign, Champaign, IL, USA, in 1971 and 1973, respectively. From 1974 to 1976, he was employed with Texas Instruments, where he worked on integrated optics. In 1976, he joined the staff of AT&T Bell Laboratories, Holmdel, NJ, USA. In Crawford Hill Laboratory, he worked on a variety of optoelectronic devices, including semiconductor lasers, optical modulators, waveguide switches, photonic integrated circuits, and photodetectors with emphasis on high-speed avalanche photodiodes for high-bit-rate lightwave systems. In January 1989, he joined the Faculty of the University of Texas at Austin as a Professor of electrical and computer engineering and Cockrell Family Regents Chair of engineering. In January 2006, he moved to the University of Virginia, Charlottesville, VA, USA, as the Lucian Carr Professor of electrical and computer engineering. Prof. Campbell's technical area is photodetectors. He is currently actively involved in single-photon-counting APDs, Si-based optoelectronics, high-speed low-noise avalanche photodiodes, and high-power high-linearity photodiodes. He has coauthored 11 book chapters, 490 articles for refereed technical journals, and more than 500 conference presentations. In 2002, he was inducted into the National Academy of Engineering.